Chem

Article

Exerting control of self-assembly pathways via morphological switching and patterning in amino-acid-based benzene-1,3,5-tricarboxamide conjugates

Graphical abstract

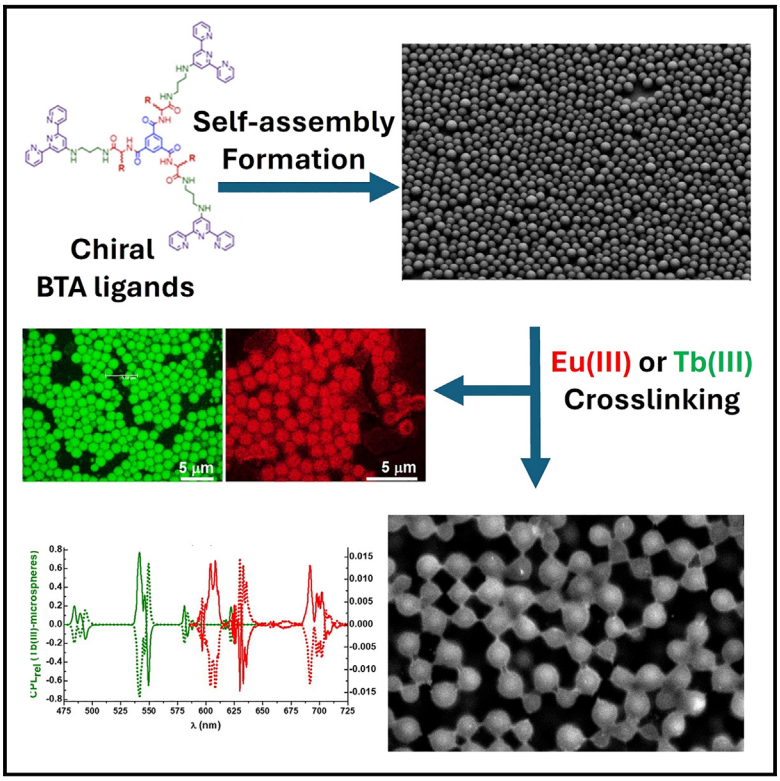

Highlights

- Different α-amino-acid-based BTAs give rise to self-assemblies with distinct outcomes
- The outcome is the formation of robust self-assembly gels and (hard) microspheres
- Hierarchical self-assembly formation is achieved by using Ln(III) crosslinking
- The chirality of the Ln-assemblies formed is probed by using CPL

Authors

Aramballi J. Savyasachi, Oxana Kotova, Ena T. Luis, ..., Robert Pal, John J. Boland, Thorfinnur Gunnlaugsson

Correspondence

robert.pal@durham.ac.uk (R.P.), jboland@tcd.ie (J.J.B.), gunnlaut@tcd.ie (T.G.)

In brief

Amino-acid-based tripodal benzene-1,3,5-tricarboxamide (BTA) ligands show the formation of self-assembly structures (two types) with distinct morphological outcomes. Using glycine results in a soft material, whereas (either *R* or *S*) alanine, phenylalanine, and leucine results in the formation of solid microspheres in aqueous solutions. The use of lanthanide ions (Ln = Eu/Tb(III)) leads to crosslinking of the chiral microspheres, with the chirality of the BTA influencing the helicity of the resulting assembly as was evident by measuring the circularly polarized luminescence (CPL) of the microspheres.

Savyasachi et al., 2025, Chem *11*, 1–12
February 13, 2025
Published by Elsevier Inc.
https://doi.org/10.1016/j.chempr.2024.09.020

CellPress

Chem

CellPress
OPEN ACCESS

Article

Exerting control of self-assembly pathways via morphological switching and patterning in amino-acid-based benzene-1,3,5-tricarboxamide conjugates

Aramballi J. Savyasachi,[1,2] Oxana Kotova,[1,2] Ena T. Luis,[1] Amy D. Lynes,[1] Shaun Mills,[1,3] Sandra A. Bright,[1,4] Gavin J. McManus,[4] Matthias E. Möbius,[2,5] D. Clive Williams,[4] Robert Pal,[6,*] John J. Boland,[1,2,3,*] and Thorfinnur Gunnlaugsson[1,2,7,*]

[1]School of Chemistry and Trinity Biomedical Sciences Institute, Trinity College Dublin, The University of Dublin, Dublin 2, Ireland
[2]AMBER (Advanced Materials and Bioengineering Research) Centre, Trinity College Dublin, The University of Dublin, Dublin 2, Ireland
[3]Centre for Research on Adaptive Nanostructures and Nanodevices (CRANN), Trinity College Dublin, The University of Dublin, Dublin 2, Ireland
[4]School of Biochemistry and Immunology, Trinity Biomedical Sciences Institute, Trinity College Dublin, The University of Dublin, Dublin 2, Ireland
[5]School of Physics, Trinity College Dublin, Dublin 2, Ireland
[6]Department of Chemistry, Durham University, South Road, Durham DH1 3LE, UK
[7]Lead contact
*Correspondence: robert.pal@durham.ac.uk (R.P.), jboland@tcd.ie (J.J.B.), gunnlaut@tcd.ie (T.G.)
https://doi.org/10.1016/j.chempr.2024.09.020

THE BIGGER PICTURE One of the grand challenges within (supramolecular/nano) chemistry is the ability of chemists to develop novel ligands that enable them to exert control over self-assembly pathways/processes in the formation of complex supramolecular nanostructures and materials. In this contribution, we aim to address this by developing benzene-1,3,5-tricarboxamide (BTA)-based supramolecular building blocks consisting of α-amino acids, a covalent spacer, and terpyridine (tpy) as a "capping" coordination building block. We show, using various experimental techniques, methods, and conditions (solvents, ions, etc.), that these building units, within competitive media, influence the self-assembly processes greatly, resulting in the controlled formation of novel structures (e.g., gels and microspheres). Furthermore, we demonstrate that "post-synthetic" modification can result in the formation of unique supramolecular structures with novel structural, morphological, and functional properties.

SUMMARY

Small structural changes to benzene-1,3,5-tricarboxamide (BTA) dictate its self-assembly behavior and morphological outcome. Functionalization with an α-amino acid close to the BTA core, which also possesses a terminal terpyridine (tpy) unit, led to a robust gel in the case of glycine, whereas monodisperse, solid microspheres formed in the case of alanine, phenylalanine, and leucine. The self-assembly pathways of the chiral and achiral BTAs are orthogonal and both microspheres and gel fibers independently assemble in the same medium. Further hierarchical self-assembly results upon addition of lanthanide ions (i.e., Eu(III) and Tb(III) that emit at long wavelengths with long excited-state lifetimes) that crosslink the microspheres through coordination, whereas coordination within the gel led to a change in morphology toward microspheres, as well as the formation of hierarchical superstructures. The chirality of the BTA influences helicity of the assembly and the resulting enantiomeric conformation around the lanthanides, evidenced by circularly polarized luminescence.

INTRODUCTION

At the nanoscale, a synthetic material's structural features are a direct result of the interplay between its component molecules. This phenomenon is at the core of self-assembled supramolecular materials.[1] The self-assembly of small building blocks can result in the formation of a wide variety of nanoscopic structures, including micelles,[2] bilayers and vesicles,[3] and one-dimensional fibers in gel-like phases,[4–6] to name a few. Exerting control over the self-assembly pathways of synthetic building blocks is highly

Please cite this article in press as: Savyasachi et al., Exerting control of self-assembly pathways via morphological switching and patterning in amino-acid-based benzene-1,3,5-tricarboxamide conjugates, Chem (2024), https://doi.org/10.1016/j.chempr.2024.09.020

challenging,[7–10] particularly because supramolecular pathways are dictated by the balance of many processes working in a synergetic manner, and are highly dependent on both structure and medium.[11] Controlling self-assembly remains a challenge that hinders the design of molecules that will deliver predictable nanoscopic structures and, in turn, dictate their macroscopic function.[12,13]

Self-assembly processes are essential to all life. Amino acids and peptides are some of the key building blocks of life, and research into synthetic self-assembly based on such entities has attracted significant interest in recent times.[14–16] Indeed, systems consisting of as few as 2–4 amino acids have been shown to generate materials, such as soft self-assembly hydrogels.[17,18] Notably, the gels possess sequence-dependent properties that are programmable via modulation of the hydrophilic and hydrophobic nature of the amino acid/peptide segments.[19,20] This strategy of controlling macroscopic properties by manipulating amino acid segments has already been extended to other synthetic building blocks.[21–23]

Recently we, and others, have focused on the use of benzene-1,3,5-tricarboxamide (BTA) structures, which are versatile building blocks, possessing three points of connectivity, for the design and the construction of tunable[24–26] and stimuli-responsive[27,28] supramolecular structures. Some of these examples demonstrate the use of BTA in the formation of discrete assemblies, such as with anions, to give cage compounds[29] or 2D materials,[25] or soft material and coordination polymers (using either *d*- or *f*-metal ions). Their versatility and ease of functionality make BTAs excellent candidates for structure-assembly studies[30,31] and for use in various applications, such as in luminescent sensing, imaging, catalysis, etc., or in the formation of soft-printable materials. However, we realized that a minor structural modification of such structures can have major influences on their self-assembly properties, both in solution and in the solid state. For example, we demonstrated that **1**, which consists of a short hydrocarbon spacer and a terminal terpyridine (tpy) unit, gives rise to the formation of a soft but fragile gel material (Figure 1A).[32] However, through *in situ* crosslinking using lanthanide ions, more robust gels were formed, which were employed to grow salt nanowires of single-crystal halide salts (e.g., NaCl, KCl, and KI) forming so-called chemical nano-gardens[33]; these possess unique morphological structures previously unreported. We have also incorporated BTAs into metallogels,[34,35] crystalline materials, gels (where we demonstrated that use of ester vs. acids, or alkyl chain lengths, can have a major effect on the self-assembly outcome, where competitive hydrogen bonding interactions can easily overwrite the formation of "classically" expected helically $\pi-\pi$-stacked BTA units),[36] and coordination polymers.[37] BTAs have also been functionalized with amino acids to program their self-assembly behavior.[38–45] Here, we demonstrate that incorporating α-amino acids into the design of structure **1**, yielding the BTA ligands **2–5** (Figure 1A) that only differ in the nature of a single α-amino acid (*Gly, Ala, Phe*, or *Leu*, respectively) enabled us to direct the formation of remarkably different hierarchical materials with distinct physical and morphological features in a manner not previously demonstrated. By using a variety organic H_2O solvent mixtures, this minor structural modification of **1** allowed us to exert control over the formation of either soft fibrous material through one-dimensional supramolecular polymerization or hard solid spherical particles in a reproducible and controllable manner. Only in the case of **2** was a one-dimensional fibrous material formed as a gel, whereas for **3–5** (*R*/*S*), the sole formation of enantiomerically pure solid spherical particles was observed. These particles could then be post-synthetically modified with lanthanide metal ions, such as Eu(III) and Tb(III) (both of which give rise to long-wavelength and long-lived "delayed" luminescence), to give higher-order and crosslinked hierarchical superstructures with unique chiral luminescent properties.

RESULTS AND DISCUSSION

Synthesis and self-assembly studies of amino-acid-functionalized BTAs

Scheme S1 summarizes the synthesis of **2–5**, which were achieved in good yields and high purity from 1,3,5-benzenetricarbonyl chloride (see supplemental information). Due to their low solubility, it was necessary to heat **2–5** at 100°C in the respective mixtures of water and organic solvent (in a sealed tube). The mixtures were slowly cooled to room temperature under ambient conditions to induce self-assembly. In the case of **2** (c = 0.5% w/v) in a 6:4 v/v CH_3CN/H_2O mixture, upon cooling to room temperature, the formation of a translucent gel was observed within 8–12 h (Figure 1B). The gelation time was decreased to 60 min at an increased concentration of 1% w/v. Scanning electron microscopy (SEM) and transmission electron microscopy (TEM) analysis of the xerogels of **2** confirmed the formation of one-dimensional fibrous structures typical of BTA-based assemblies (Figures 1C and 1D). These gels were thermally and mechanically reversible, yet significantly robust. Rheological measurements demonstrated that the 0.5% w/v gel possessed self-healing properties, with a fast recovery time of ~30 s (Figure 1E). For the rheological characterization of this sample, we recorded two subsequent runs, each consisting of an oscillatory rheology test and a recovery test. The moduli of the strain and frequency sweeps (Figures S11A and S11B) are averaged over two subsequent measurements and show good reproducibility. The gel exhibits yielding and weak frequency dependence of the moduli which is typical for gels. During the first recovery test (Figure S11C), we observed a steady decrease of the moduli, which did not recover to their original values as shown by the subsequent strain sweep (Figure S11D). In principle, this could be either due to changes in the gel microstructure (aging) or sample evaporation that is difficult to fully avoid even with the solvent trap making the sample more concentrated on one hand but also reducing the amount of sample between the plates. However, because the moduli during the second recovery test (Figures 1E and S11E) are stable over time, it suggests that the initial decrease of the moduli is due to a strain-induced change of the microstructure rather than evaporation, which would lead to a continuous change of the moduli that is not observed.

We also studied the effect of the concentration on the gelation properties and made gels of **2** at 0.5%, 1.0%, 1.5%, and 2.0% w/v in 6:4 v/v CH_3CN/H_2O solution (Figure S12A). In the case of 0.5% and 1.0% w/v, the formation of fibril network was observed (Figures S12B and S12C) that was corresponding to

Please cite this article in press as: Savyasachi et al., Exerting control of self-assembly pathways via morphological switching and patterning in amino-acid-based benzene-1,3,5-tricarboxamide conjugates, Chem (2024), https://doi.org/10.1016/j.chempr.2024.09.020

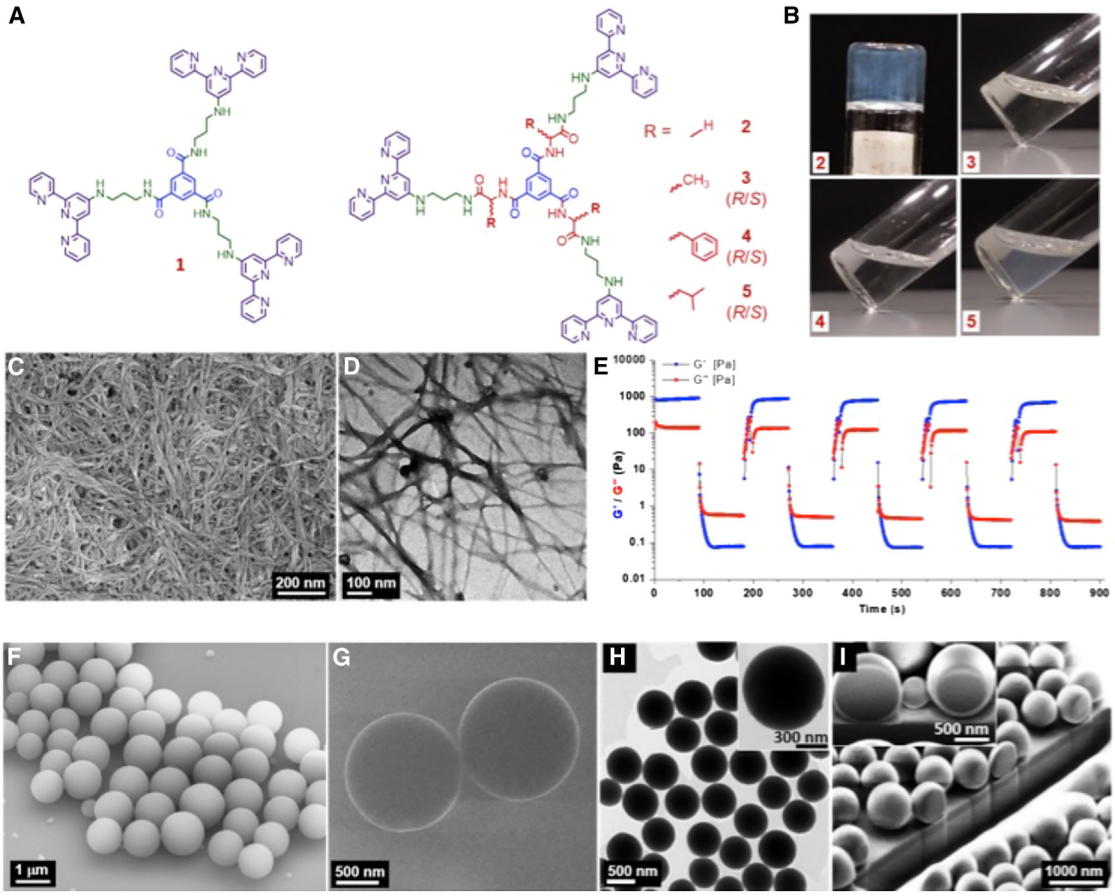

Figure 1. Morphological changes of self-assembled tripodal BTA molecules

(A) Schematic representation of the BTAs before and after encoding stereogenic centers onto **1** using selected amino acids yielding **2**–**5**.

(B) Images of **2**–**5**.

(C) SEM image of the xerogel formed from **2** (0.5% w/v in 6:4 v/v CH_3CN/H_2O).

(D) TEM image of the xerogel formed from **2** (1% w/v).

(E) The recovery test performed on gel **2** (0.5% w/v).

(F and G) (F) SEM and (G) helium ion beam (HIB) microscopy images of self-assembled microspheres formed from (*S*)-**3** (0.2% w/v).

(H) TEM images of the (*S*)-**3** microspheres; inset: magnified image showing its solid internal structure.

(I) SEM image of (*S*)-**3** microspheres showing precise cut using focused ion beam (FIB) technique.

the 0.5% w/v microstructure shown in Figures 1C and 1D for the SEM and TEM images, respectively. For 1.0%, 1.5%, and 2.0% w/v gels formed in the same 6:4 v/v CH_3CN/H_2O solution, a clear precipitation began to occur, possibly due to limited solubility at this higher concentration. This result led us to probe the effect of the solvent where gels of **2** were also formed when using 1% w/v in $MeOH/H_2O$ and $EtOH/H_2O$ solvent mixtures. The SEM images of these also demonstrated the formation of fibrous networks (Figures S12D and S12E) of similar nature to that seen for the CH_3CN/H_2O solution demonstrating the variety of polar solvents that may be used for gelation. We also attempted to form gel from **2** in 1% w/v in *i*-$PrOH/H_2O$. However, this sample did not sustain the reverse sample test; but SEM imaging also showed the formation of a fibril network similar to the other solvent mixtures (Figure S12F).

Although the simple modification of **1** by inserting a glycine moiety resulted in soft material formation for **2**, then as shown below, the nature of the α-amino acid side chain significantly impacts the final assembly (Table S2). In contrast to **1** and **2**, compounds (*R*/*S*)-**3**–**5** did not yield gels using similar aqueous mixtures with CH_3CN, MeOH, EtOH, *i*-PrOH, DMSO, and DMF. This is demonstrated in Figure 1B for the CH_3CN/H_2O mixture, where no gelation was observed as had been for **2**. However, all the samples were drop casted onto silica wafers and analyzed using SEM and helium ion beam (HIB) microscopy after drying (Figures 1F–1I). In stark contrast to that seen for **2**, these analyses demonstrated the formation of spherical particles, possessing smooth surface and uniform size distribution. Of these, **3** (0.2% w/v in 6:4 v/v CH_3CN/H_2O) showed the most highly monodisperse particle size distribution in the range of 0.8–1.1 μm diameter (mean particle size of 0.97 ± 0.08 μm, Figures 1F–1I). Increasing the concentration resulted in polydisperse microspheres, and above 0.5% w/v, the formation of precipitate was observed. Hence, for further analysis, the

Please cite this article in press as: Savyasachi et al., Exerting control of self-assembly pathways via morphological switching and patterning in amino-acid-based benzene-1,3,5-tricarboxamide conjugates, Chem (2024), https://doi.org/10.1016/j.chempr.2024.09.020

concentration of the sample was maintained within 0.2%–0.4% w/v. Furthermore, the morphology and the size distribution of these microspheres was shown to be highly influenced by the solvent systems (Table S3), demonstrating the importance of the local environment in the self-assembly processes. When **3–5** (0.2% w/v) were prepared in aqueous 1:1 v/v mixtures with CH_3OH, microspheres with 1–1.5 μm diameter formed along with smaller ones, whereas the mixtures with EtOH or *i*-PrOH resulted in polydisperse microspheres with an average diameter of 500 nm. Further, the mixtures with THF led to fused particles, whereas the addition of 1,4-dioxane revealed no particle formation. Therefore, it can be concluded that CH_3CN/H_2O ensures the appropriate balance between hydrophobicity and hydrophilicity toward the compounds **3–5** to ensure the formation of monodisperse microspheres. The remaining discussion will mainly focus on the self-assembly of **2–5** in 6:4 v/v CH_3CN/H_2O media.

The microspheres formed from **3–5** were characterized extensively by microscopy and proved to retain their structure during various imaging processes. The microspheres were found by SEM to be thermally stable until 155°C without showing any deformation in their spherical shape, whereas within the range of 160°C–165°C, the microsphere structure was lost due to their melting because this temperature corresponds to the melting points found for compounds **3–5** within experimental errors (see supplemental information and Figure S16). Thermogravimetric analysis (TGA) showed thermal chemical decomposition at a range of 317°C–326°C. TEM analysis was also performed to investigate the internal structures of these microspheres, but the particles did not allow the electron beam to pass through the samples, indicating that the microspheres were solid inside. This was confirmed using focused ion beam (FIB) in combination with SEM (Figure 1I). The particles were also analyzed using atomic force microscopy (AFM)-Raman spectroscopy; the Raman mapping confirmed the results previously seen in SEM, TEM, and HIB analysis (Figure S18). The AFM size distribution analysis revealed that upon increasing the concentration (in this case of **3**) from 0.1% to 0.5% w/v, the average size distribution of the microspheres increased from 0.52 ± 0.07 to 0.85 ± 0.19 μm, corroborating with related SEM studies (Table S5). Mechanical measurements using AFM further supported the above size distribution, whereas mechanical strength measurements also confirmed the solid-state nature of these particles. Using the AFM cantilever, the particles could be moved through lateral force displacement measurements, demonstrating that they were not adhered to the silica substrate. In fact, the particles could be easily transferred from the substrate using a micrometer-sized needle with the help of static force of interaction. When lateral force was applied to (*S*)-**3** microspheres using the AFM cantilever, an initial force of 0.48 μN was required to move the particle, being displaced ~300 nm from their initial position; the force required to push the particle was subsequently reduced to ~0.1 μN (Figure S20). Being purely organic single-component self-assembled particles, these freestanding, solid microspheres are similar to those observed for metallic or coordination network nanoparticles[46–49] and polymer nanospheres.[50,51] The unexpected formation of hard microspheres demonstrates that a subtle structural change induced by the presence of the hydrophobic amino acid completely alters the self-assembly pathways of these BTA building blocks.

Characterization of microsphere formation

To acquire insights into the pathway of the assembly process during the formation of the microsphere, systematic studies in solution were undertaken. Initially, we examined the variation in the characteristic photoluminescent properties of **3** using 6:4 v/v CH_3CN/H_2O solvent media at room temperature (Figure S25). At low concentrations (5×10^{-6} M), only the monomeric emission of **3**, centered at 413 nm (λ_{ex} = 280 nm) was observed. Upon increasing the concentration of **3** (to 3×10^{-4} M), the emission intensity reached a maximum at ~1×10^{-5} M; thereafter, it was quenched, and a second red-shifted emission band appeared, assigned to the formation of a self-assembled structure. We also monitored the emission spectra upon excitation at 405 nm, which would populate only the excited state of the newly formed self-assembly in solution. Indeed, here, an emission band centered at *ca.* 490 nm was observed; the excitation spectra showed the formation of a species consisting of two main bands at 350 and 405 nm. Furthermore, the circular dichroism (CD) spectra were also recorded at different concentrations (5 μM → 1 mM). Unfortunately, such as in the case of **3**, the quality of the spectra was poor (*cf.* (*R*)-**3** in Figure S28), and although we did observe bisignated Cotton effect upon increasing concentration (which would support the helical formation between the ligands), further analysis of these changes was not feasible due to the poor quality of the spectra. Nevertheless, such low CD- response could indirectly be the consequence of the formation of the microspheres at higher concentration.

Laser scanning confocal microscopy (LSCM) imaging of isolated microspheres resulted in emission centered at λ_{em} = 492 nm, matching that seen of these microspheres in solution. We also used LSCM to monitor the self-assembly of **3** in real time.[52] A freshly prepared hot solution of **3** (c = 0.2% w/v) in 6:4 v/v CH_3CN/H_2O (50 μL) was placed onto a closed quartz Petri dish, and while the solution cooled, time-lapse imaging was performed, Figure 2 (λ_{ex} = 405 nm, the real-time videos are given in the supplemental information).

Upon initial cooling, the formation of premature luminescent aggregates was observed (at *ca*. t = 4.40 min in Figure 2, top), which we attributed to an initial stage of aggregation of **3**. Almost immediately thereafter, the assemblies grew in an anisotropic manner, resulting in the formation of the microspheres (*cf.* beyond *ca*. t = 5.30 min in Figure 2, top). These microspheres were isolated and imaged using SEM and were found to be identical to those produced above and shown in Figure 1. Furthermore, by tuning the solvent media, we were able to accelerate this assembly process in real time (Figure 2, bottom). This allowed us to investigate using SEM the stepwise formation of the particles by preparing a series of samples of **3** (0.2% w/v), formed using decreasing CH_3CN/H_2O ratios (10:1→1:10) at 80°C, followed by cooling and lyophilizing at −40°C. Gratifyingly, the lyophilization process resulted in the formation of clusters of aggregated materials of different nanodimensions. These consisted of fused nanoparticles (or nanoseeds) that were shown to form higher-order hierarchical structures, or initial particles, which we classified as meta-stable aggregates. The latter were

Please cite this article in press as: Savyasachi et al., Exerting control of self-assembly pathways via morphological switching and patterning in amino-acid-based benzene-1,3,5-tricarboxamide conjugates, Chem (2024), https://doi.org/10.1016/j.chempr.2024.09.020

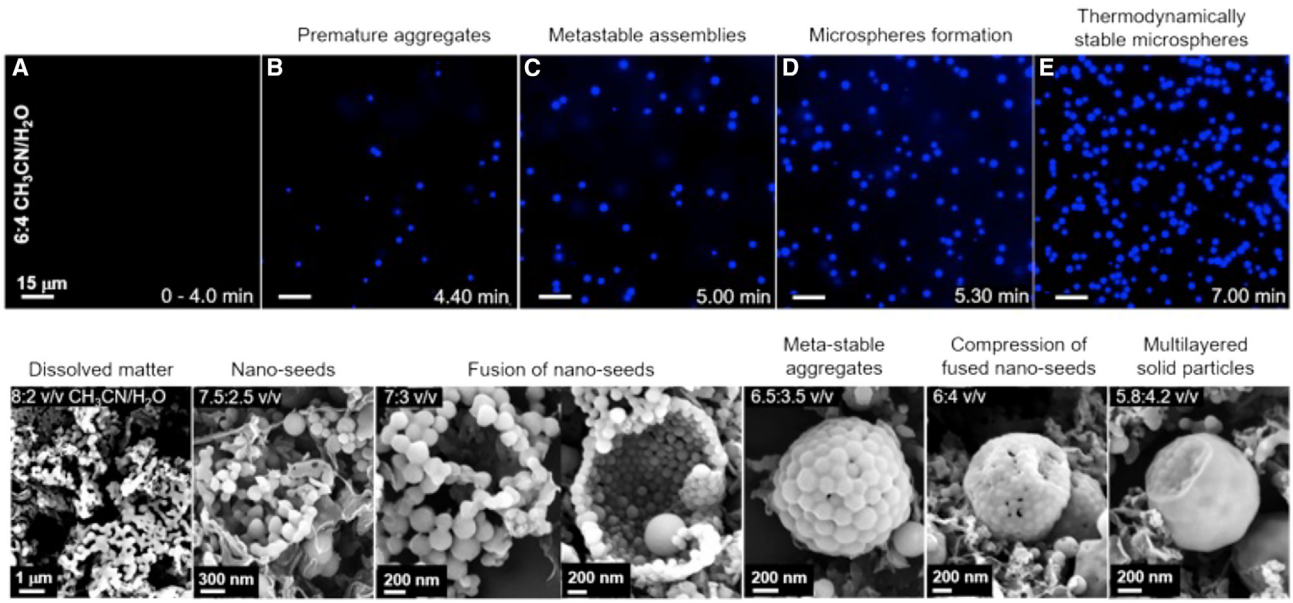

Figure 2. Real-time investigation of the assembly evolution

Top: LSCM snapshots taken from Video S1 (A–E) at different time intervals upon cooling the hot solution of (*S*)-**3** (c = 0.2% w/v, 50 μL) in 6:4 v/v CH_3CN/H_2O with λ_{ex} = 405 nm and emission window 414–721 nm. Bottom: snapshots of the stepwise microparticle formation. SEM images of the powder obtained from lyophilizing a series of solutions of (*S*)-**3** in different CH_3CN/H_2O ratios (10:1 → 1:10) showing the intermediate stages of aggregation process occurring in the formation of microparticles.

closely packed, eventually forming solid material, consisting of internal core packing of multi-layered self-assembled nanoparticles (Figure 2, bottom). The driving force for their self-assembly formation is very likely through a nucleation-elongation model established for supramolecular polymers,[53] forced by intermolecular hydrogen bonding interactions, $\pi-\pi$ stacking, and hydrophobic effects. Of these, the latter is clearly highly important and possibly a dominating factor for (*R*/*S*)-**3**–**5**, giving the strikingly different morphological and physical outcome to that seen for **2** under the same experimental conditions. Hence, the simple introduction of hydrophobic moieties close to the central BTA core gives a handle to enable control between the two self-assembly pathways with distinctive morphological outcomes. Importantly, the process was found to be independent of the stereochemistry of the amino acids used because both *R* and *S* enantiomers resulted in the formation of the hard microparticles of **3**. These results would indicate that the nature of the solvent is important but that the overall self-assembly driving force in the CH_3CN/H_2O mixtures is due to hydrophobicity, hydrogen bonding, and $\pi-\pi$ stacking and not due to for instance, protonation of the tpy units.

To further probe the driving force for self-assembly, we carried out an experiment where we mixed **2** with (*R*/*S*)-**3**–**5**, in the ratios of 5:1.5, 3:1, or 4:1, in the 6:4 v/v CH_3CN/H_2O media, in the hope to observe self-sorting. Indeed, this was found to be the case because a fibrous gel network was obtained along with the particles (Figures 3A–3C).

This demonstrates the co-existence of the two independently self-assembled species (i.e., **2** and **3**, **4**, or **5**) in the same medium within 24 h. However, these particles were shown to be smaller, around 200–500 nm in size, compared with those formed above, demonstrating the potential application of the gel to access alternative particle size distributions. These experiments showed that there was a self-sorting phenomenon occurring, where compound **2** formed the expected gel structure, and compounds **3**, **4**, or **5** all formed particles. Hence, this would indicate that there is no select co-assembly formation between these ligands upon mixing with gelator **2**.

The microspheres formed from **3** and **5** were found stable over a period of time as was clear from their SEM images with no morphological changes observed over a period of months in the 6:4 v/v CH_3CN/H_2O medium. However, in the case of **4**, we noticed the formation of elongated fibrous networks in this medium after 7 days, indicating a morphological switching from microparticles to soft matter. After 4 weeks, the dominant presence of the soft matter was observed, the SEM imaging of which indicated strong similarity to that seen for **2** above (Figures 3D–3I). Although this is a long time period, it does demonstrate that the hydrophobic nature of the amino acid has a strong effect on the stability and the final outcome of the self-assembly process. This prompted us to investigate if the structure of the particles could be modified using a procedure similar to protein denaturation by chaotropic denaturants, such as urea. Indeed, such a disassembling process was observed but only in treating the particles with 6 mol equiv of urea and only after 4 h (other concentrations/equiv were used, but only at 6 mol equiv did we observe the "denaturation"). The morphology changed from the well-defined and dispersed particles into a "liquid"-like material, demonstrating that urea was able to interact with the assembly, causing morphological changes. This is an important

Please cite this article in press as: Savyasachi et al., Exerting control of self-assembly pathways via morphological switching and patterning in amino-acid-based benzene-1,3,5-tricarboxamide conjugates, Chem (2024), https://doi.org/10.1016/j.chempr.2024.09.020

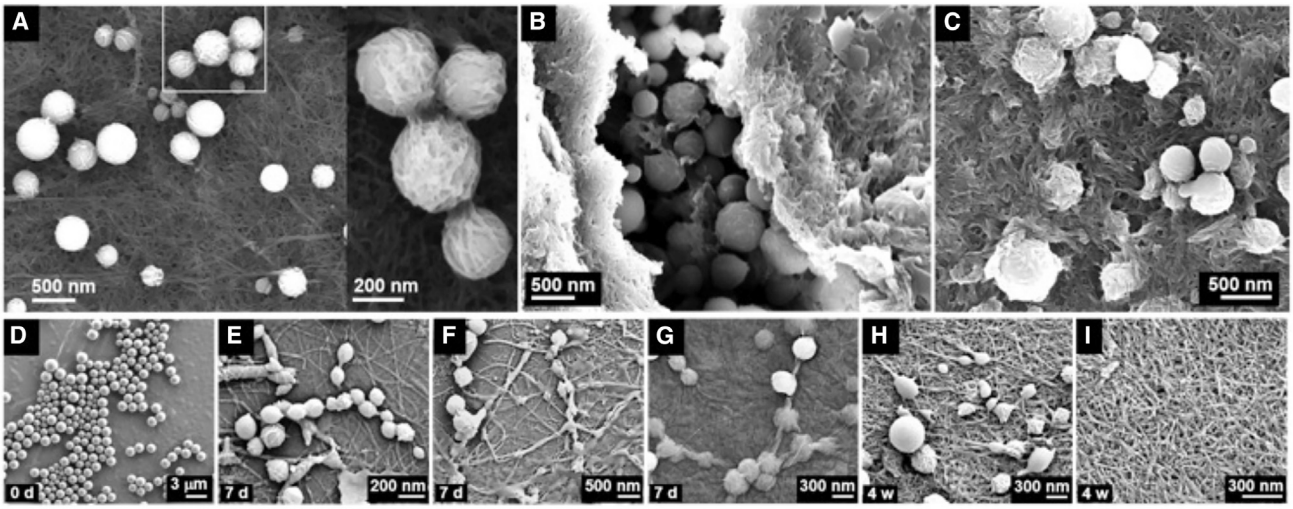

Figure 3. Self-sorting of BTA molecules and aging of microspheres

(A) SEM image of mixed **2**:(*S*)-**3** translucent gel (3:1 ratio, 0.3% w/v gelator) showing the co-existence of the two independently self-assembled species in the same medium, elongated gel fibers and spherical microparticles; expanded image shows the microspheres wrapped with gel fibers.

(B and C) SEM images of **2**:(*S*)-**4** gel and **2**:(*S*)-**5** gel (4:1 ratio, 0.4% w/v gelator) showing the embedded microspheres distributed all over the gel matrix; microspheres observed at the surface and few layers beneath the gel network.

(D–I) SEM images of the dropcasted solution of microspheres of **4** at different time intervals showing the switching of morphology from spherical microparticles to elongated fibrous structures over a period of 4 weeks.

observation, given the importance of the hydrogen bonding interactions in the formation of the microsphere.

We also attempted to synthesize these organic microparticles in the presence of urea. Importantly, using 1–3 mol equiv of urea showed no effect on their formation. However, at 4–5 mol equiv of urea, deformed microspheres were obtained, whereas at 6 mol equiv no microsphere formation occurred. We also monitored this disassembly in real time using LSCM imaging by using isolated microspheres of **3**, the process occurring over 6 h. When the same experiment was repeated using an excess of urea with **2**, the self-supporting nature of the gel was removed, indicating that the self-assembly was also interrupted by the competitive hydrogen bonding of urea. This indicates that under certain conditions, urea denatures the self-assembly by overcoming the hydrogen bond network and the hydrophobicity imbued by the amino acid functionalization within (*R/S*)-**3**–**5** molecules (see supplemental information, Figures S29 and S32–S35; Tables S8–S10).

Crosslinking of microspheres with lanthanide ions: Formation of long-lived luminescence materials

We next explored the possible formation of hierarchical superstructures from the particles[54] through lanthanide crosslinking by binding of the metal ions to the tpy chelating sites on each ligand. We employ the term "crosslinking" herein to describe the macroscopic interaction observed between particles, which is driven by the lanthanides, leading to a "pseudo" crosslinking between them. It was necessary to carry these investigations out at relatively high concentration of 1.55 mM of particles. Hence, it was not possible to record their absorption spectra. However, the emission from both the ligand and Ln(III) center were monitored (see supplemental information, Figures S38–S44), which allowed to determine the appropriate amount of Ln(III) ions (Ln = Eu and Tb) required to obtain luminescent microspheres with maximum emission intensity at ~1 equiv.

In the case of the particles, either Eu(III) or Tb(III), both of which are commonly used in the formation of luminescent materials, were added (1 mol equiv) to a solution of preformed microparticles of **3** (0.4% w/v) in 6:4 v/v CH_3CN/H_2O. The resulting solution was left to equilibrate for 1 h, followed by dropcasting onto silica substrate and drying. The SEM results (Figure 4B) demonstrated the formation of closely interconnecting or crosslinked particles, with an average distance and thickness of 90 ± 20 and 100 ± 25 nm, respectively, for both lanthanides. By altering the concentration (e.g., 0.1 %–0.4 % w/v) of **3**, we were able to control the degree of crosslinking in these particles, enabling the arrangement of these microspheres into linear or grid-like structures (Figure S45). The formation of such interconnected particles was observed when using various EuX_3 salts (X = CF_3SO_3, CH_3COO, Cl, NO_3, and ClO_4) and the obtained crosslinked (*S*)-**3**-Eu(III) microstructures are represented on Figure S46. The energy dispersive X-ray (EDX) microanalysis of these crosslinked particles revealed the presence of the lanthanide ions along the surface of the particle's chains. The X-ray fluorescence spectrum showed peaks at 5.84 (L_α) and 1.13 (M_α) keV responsible for the X-rays emitted from the L and M shells in the case of Eu(III) and the elemental composition indicated the presence of 5.6% of Eu(III) on the sample surface (Figures 4D and S50). Similar results were seen for Tb(III) (Figure S51).

The photoluminescence of these crosslinked particles was also probed in 6:4 v/v CH_3CN/H_2O solution. Characteristic lanthanide emission was observed, which, in the case of Eu(III), occurred at 580, 595, 617, 652, and 697 nm ($^5D_0 \rightarrow {}^7F_J$ transitions; J = 0–4), indicating coordination of the lanthanide ions to

Please cite this article in press as: Savyasachi et al., Exerting control of self-assembly pathways via morphological switching and patterning in amino-acid-based benzene-1,3,5-tricarboxamide conjugates, Chem (2024), https://doi.org/10.1016/j.chempr.2024.09.020

CellPress
OPEN ACCESS

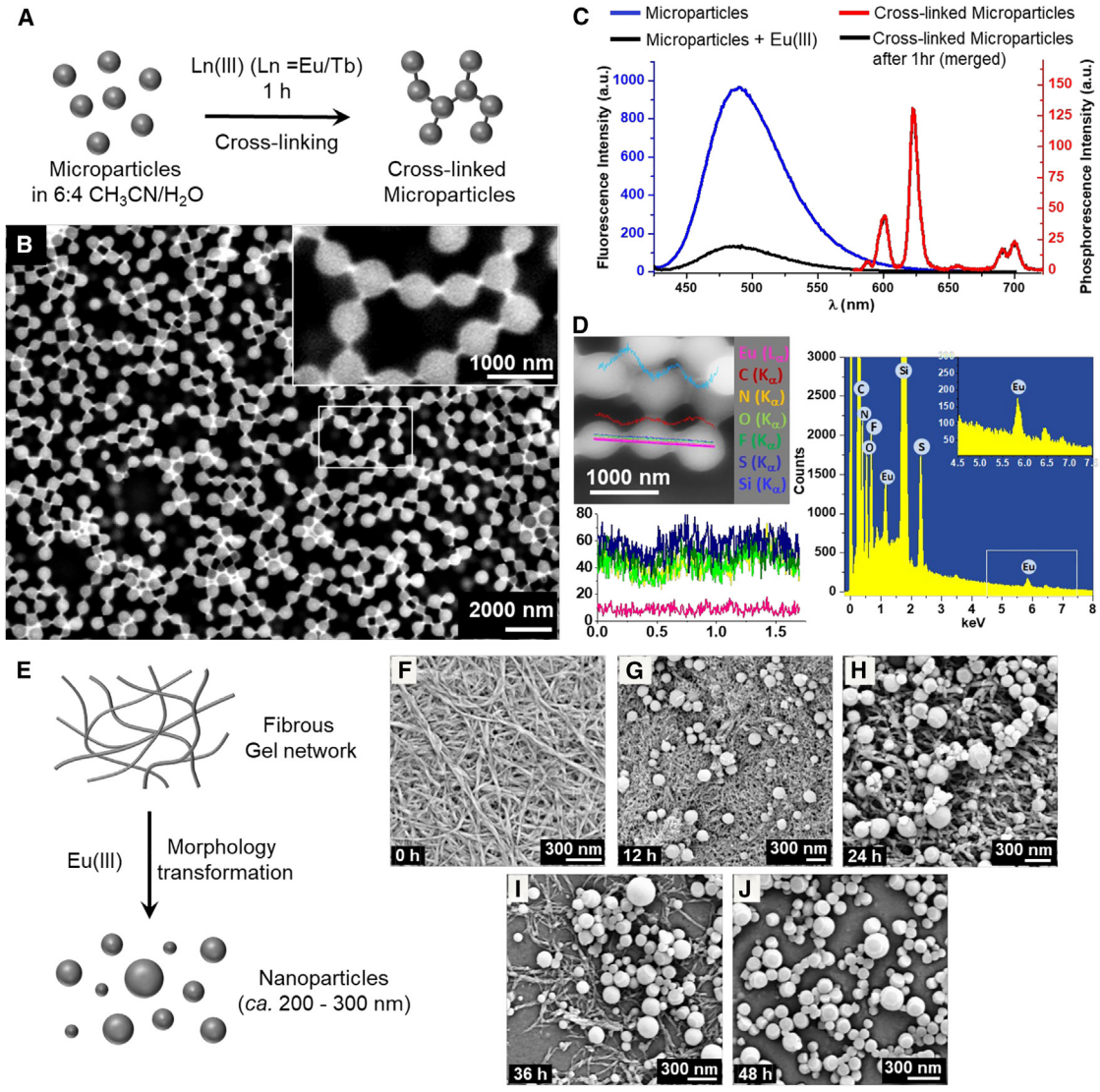

Figure 4. Hierarchically crosslinked microparticle superstructures via Ln(III) coordination

(A) Preparation of crosslinked microparticles.

(B) The SEM image of the crosslinked elongated microsphere chains formed on addition of $Eu(CF_3SO_3)_3$, to a solution of (*S*)-**3** microspheres (0.4% w/v).

(C) Fluorescence spectrum showing the emission from (*S*)-**3** microparticles (λ_{ex} = 405 nm, blue) being quenched after the addition of Eu(III) (black and red, λ_{ex} = 380 nm).

(D) SEM image of the EDX analysis (line scan mode) performed on the crosslinked microparticles showing the presence of Eu(III) along the surface and the X-ray fluorescence spectrum showing the X-ray peaks at 5.84 (Λ_α) and 1.13 (M_α) for Eu(III) (see Figures S50 and S51 for more details on crosslinked microspheres formed with $Tb(CF_3SO_3)_3$).

(E) Schematic representation of the morphology transformation of fibrous gel network of **2** to spherical nanoparticles upon Eu(III) diffusion.

(F–J) SEM images showing the transformation of the one-dimensional fibers to nanoparticles at different time intervals.

tpy groups on the surface of the microspheres (Figures 4C and 5E). These materials were photostable upon continuous monitoring over 12 h, which indicated stable lanthanide-mediated crosslinking (Figures S49B and S52).

Using the same synthetic procedure, but now aging the resulting Ln(III) samples for only 10 min under agitation, led to only isolated particles of **3**. Upon excitation, these particles also gave rise to typical lanthanide emission spectra with lifetimes of 1.4 and 0.5 ms, for Eu(III) and Tb(III), respectively (see the following section for detailed description). The observed luminescence demonstrates that agitation prevents crosslinking between microspheres, but the interaction with Ln(III) ions with tpy is still occurring, demonstrating that two different mechanisms, possibly due to different equilibrium processes, are taking place under these experimental conditions but both involving coordination of the lanthanides at the surface of the particles.

We next investigated the effect of diffusing a solution of Eu(III) into a freshly made fibrous gel of **2** (in 6:4 v/v CH_3CN/H_2O). This

Please cite this article in press as: Savyasachi et al., Exerting control of self-assembly pathways via morphological switching and patterning in amino-acid-based benzene-1,3,5-tricarboxamide conjugates, Chem (2024), https://doi.org/10.1016/j.chempr.2024.09.020

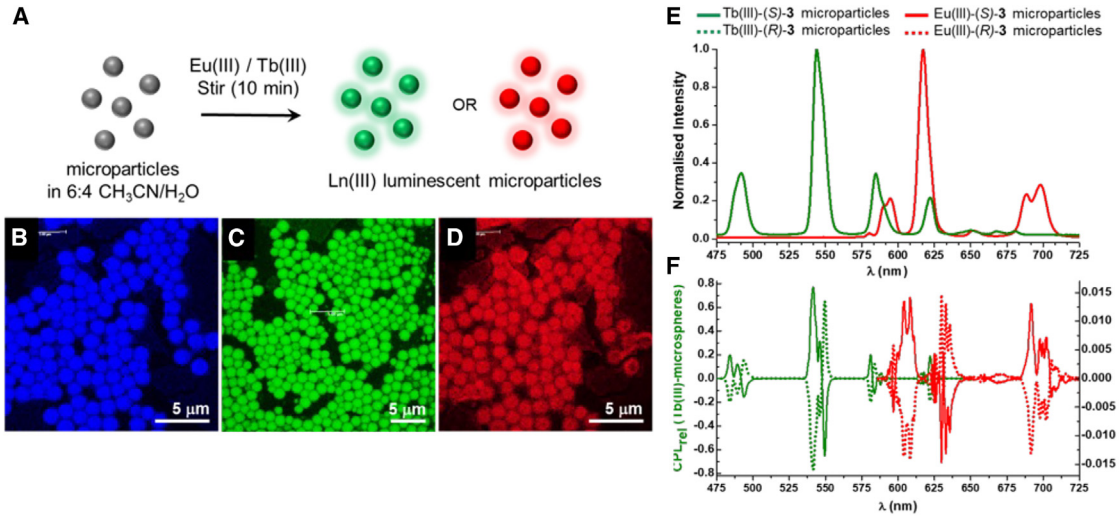

Figure 5. Interaction of Eu(III) and Tb(III) with microspheres containing a chiral BTA molecule

(A) Preparation of Eu(III) and Tb(III) based luminescent microspheres.

(B–D) LSCM images showing (B) the blue autofluorescence from Ln(III)-(*S*)-**3** microspheres (emission window 390–450 nm), (C) green emission from Tb(III)-(*S*)-**3** microspheres (emission window 450–520 nm), and (D) red emission from Eu(III)-(*S*)-**3** microspheres (emission window >570 nm).

(E) Time-gated emission spectra of Tb(III)-(*S*)-**3** microspheres (green) and Eu(III)-(*S*)-**3** microspheres (red), λ_{ex} = 365 nm taken using an epifluorescence microscope adapted for time-gated spectroscopic measurements.

(F) Time-resolved circularly polarized luminescence spectra showing the relative circularly polarized luminescence from (*R*)- and (*S*)-Tb(III)-**3** microspheres (green) and Eu(III)-**3** microspheres (red) dispersed in CH_3CN (1,000 avg. spectra, t(ex) = 1 ms, t(gate) = 20 μm and t(acq.) = 1 ms).

caused the gel to lose its robustness over time, and the original soft material (which was previously stable for months in this media) was transformed into a viscous liquid after 48 h at room temperature. SEM imaging of this sample at different time intervals showed that no morphological change occurred within the first few hours, then after 12 h of lanthanide diffusion, nanosized particles of *ca.* 200–300 nm size appeared (Figures 4E–4J). This morphological transformation process continued, and after 48 h, only nanoparticles were present. These nanoparticles also gave rise to lanthanide-centered emission upon excitation. This process is fundamentally different to that seen above in the case of **3**, where only crosslinked particles were observed, and it demonstrates our ability to direct or tune in some ways the self-assembly pathways of these BTA ligands through careful engineering, and consequently, the morphological outcome.

Probing the lanthanide-centered emission using LSCM and CPL from the hierarchical microparticle superstructures

Because **3**–**5** were formed as both *R* and *S* enantiomers, we foresaw that the self-assemblies of these will also be chiral. It should be noted that, in this case, the particles did not form the closely interconnected or grid-like structures because the interaction of the microspheres with Ln(III) ions in this case occurred only on their surface due to such interaction being performed under agitation for 10 min. This kept the particles apart from each other while still allowing for the interaction of Ln(III) ions with tpy moieties available on the surface of the microspheres. Expanding on the optical activity of luminescent Ln(III)-microspheres, we performed time-resolved circularly polarized luminescence (TR-CPL) measurements[55] to confirm the helical arrangement of molecules in the microspheres and the transfer of enantiomeric conformation to Ln(III) ions through coordination.[56–58] Prior to doing so, we measured the emission properties of the microspheres, formed using Eu(III) and Tb(III), Figure 5A, which were imaged using LSCM, Figures 5B–5D. From these figures, it is clear that these particles give rise to lanthanide-centered emission and that the fluorescence emission (from the ligand) could also be observed; hence, the blue ligand, the red Eu(III), and the green Tb(III) emission are all observed as demonstrated in Figures 5B–5D, respectively. The time-gated emission spectra from these particles were also measured using an epifluorescence microscope, which was adapted for time-gated spectroscopic measurements, Figure 5E. Further proof for the selective lanthanide coordination, stability, and the emission arising from the resulting particles (see Figures S53 and S54 in supplemental information) was observed by overlapping these different channels with images recorded using optical microscopy. Moreover, we also generated samples, where mixture of Eu(III) and Tb(III) were used (prepared as above), and these samples were imaged in identical manner. As expected, here, the two emission channels gave rise to Eu(III)- and Tb(III)-centered emissions selectively, demonstrating that the resulting particles had a mixture of these two lanthanides (see supplemental information, Figures S55 and S56). Moreover, overlapping the red and the green channels gave rise to orange emission, as indicated, visually and on a CIE (chromaticity diagram; see supplemental information, Figures S55E, S55H, and S56), this was confirmed by using both steady-state and time-gated emission spectroscopy and microscopy. By combining all three channels, the blue emission contribution could also be included, resulting in the formation of particles emitting with off-white emission, Figures S55D

Please cite this article in press as: Savyasachi et al., Exerting control of self-assembly pathways via morphological switching and patterning in amino-acid-based benzene-1,3,5-tricarboxamide conjugates, Chem (2024), https://doi.org/10.1016/j.chempr.2024.09.020

and 56D. These measurements confirm the potential application of such lanthanide-based microspheres as luminescent materials showing tunable and time-gated emission with CPL response for use in imaging and luminescent device applications.

The relative CPL (CPL_{rel}) spectra for both (*R*)- and (*S*)-Tb(III)- and Eu(III)-**3** microspheres were obtained from TR-CPL measurements.[55] These were initially measured using the 6:4 v/v CH_3CN/H_2O-mixture-prepared samples; however, although CPL was observed for both, the signal was weak; hence, it was necessary to carry these out in neat CH_3CN, where the signal was much stronger, as is evident from Figure 5F. The CPL_{rel} spectra of the corresponding enantiomers were mirror images of each other, with each spectrum showing the positive and negative signals of equal magnitudes for each lanthanide-centered emission band (Figure 5F). All major bands responsible for $^5D_{0/4} \rightarrow {}^7F_J$ (J = 6-3/0–4) transitions were symmetrically split, which corresponds to the influence of the coordination-locked geometry of the Ln(III) on the component vectors of the transitions.[59]

In the case of (*R*)- and (*S*)-Tb(III)-**3** microspheres, significant differences were observed for $^5D_4 \rightarrow {}^7F_6$ and $^5D_4 \rightarrow {}^7F_5$ transitions, which were split into three major peaks such that they crossed the x axis, and the central bands were negative. This symmetrical distribution of the CPL_{rel} signals indicates that the geometry of the Tb(III) was specifically directed by the chirality of the self-assembled microspheres, resulting in either Δ or Λ configurations of the metal center.[60] Similarly, (*R*)- and (*S*)-Eu(III)-**3** microspheres also resulted in CPL_{rel} spectra, which display the mirror image of the Eu(III)-centered emission signals for $^5D_0 \rightarrow {}^7F_{0\text{-}4}$ transitions (Figure 5F). Among them, $^5D_0 \rightarrow {}^7F_{1,2}$ and $^5D_0 \rightarrow {}^7F_4$ transitions showed the maximum intensity and were resolved into 2, 3, and 6 peaks, respectively, which could be consistent with the trigonal symmetry class.[61] However, the splitting in any of the transitions did not cross the x axis, unlike that observed for Tb(III)-**3** microspheres.

For both Tb(III)- and Eu(III)-microspheres, the differences in the CPL signs are unique to the nature of the transitions in the specific metal configuration. However, the standard examples for the structural fingerprint of similar self-assemblies are not reported as discussed above, and this is the first example of the CPL_{rel} for Ln(III)-based microspheres obtained from TR-CPL. Table S12 lists dissymmetry factor (g_{lum}) values for Ln(III)-**3** microspheres. These measurements confirm the enantiomeric purity of the microspheres formed from both the *R* and *S* enantiomers of Tb(III)- and Eu(III)-**3**. The higher g_{lum} values observed for Tb(III)-**3** microspheres reflect more efficient sensitization of the Tb(III) emission by the ligand **3**. In the case of Eu(III), the sensitization was less efficient, leading to lower g_{lum} values. Therefore, this result gave strong evidence for the formation of helical self-assemblies of the ligands during the formation of microspheres, shown by the transfer of chirality to the lanthanide metal centers that lead to a strong CPL signal. Although aggregated or solid-state samples often suffer from emission quenching, we have shown that the lanthanide-centered CPL is preserved and possibly enhanced by the higher-order organization and demonstrated a method of functionalizing assembled microspheres with CPL for chiroptical applications. Moreover, it should be noted that, although there are works on the development of luminescent Ln(III)-containing gels containing tpy and chiral centers, the measurements of CPL for such samples is unique.[62]

Conclusions

Our work has demonstrated that the self-assembly pathways in simple organic building blocks can be tuned and controlled by using encoded amino acids within a BTA structure, which results in the formation of novel materials with highly distinct morphological and physical properties, from the same solvent medium. This demonstrates the key role that the nature of the amino acid plays in directing the self-assembly processes within such building blocks. In our case, altering the amino acid results in either robust, self-healing gels or solid, monodisperse microspheres. We further demonstrate that the outcome of the self-assembly process gives rise to long-term stable supramolecular outcomes (as in the case of **2**, **3**, and **5**), and these can be further modulated or programmed into other structures through post-synthetic engineering, such as addition of lanthanide ions that resulted in a morphological transformation from a fibrous gel to nanospheres in the case of **2** and in the formation of hierarchical crosslinked superstructures in the case of **3**–**5**. The inherent chirality of the self-assembled structures influenced the chirality of the crosslinking lanthanide ions, demonstrated by CPL measurements. We are continuing to explore the influence of small variations in BTA derivatives on self-assembly processes and their resulting luminescent hierarchical assemblies.

EXPERIMENTAL PROCEDURES

Materials and methods

General synthetic procedures

All solvents and chemicals were purchased from commercial sources and used without further purification. Flash column chromatography was performed using a Teledyne Isco CombiFlash Rf 200 automated purification system. Analytical thin layer chromatography (TLC) was performed using silica plates with aluminum backings (250 μm with indicator F-254). Compounds were visualized under UV light (254 and 365 nm). Water was purified using a Millipore Milli-Q water purification system. ^1H and ^{13}C NMR spectra were recorded on an Agilent DD2/LH spectrometer at 400 and 100 MHz, respectively. Chemical shifts are reported in ppm using deuterated chloroform ($CDCl_3$) as the solvent of record and are referenced against the solvent peak. The following abbreviations have been used for multiplicity assignments: "s" for singlet, "d" for doublet, "t" for triplet, and "m" for multiplet. Mass spectrometry was carried out using high-performance liquid chromatography (HPLC)-grade solvents. Electrospray mass spectra were determined on a Micromass LCT spectrometer and high-resolution mass spectra were carried out on a MALDI-Q-TOF-Premier (Waters Corporation, Micromass MS technologies, Manchester, UK) and high-resolution mass spectra were performed using Glu-Fib with an internal reference peak of *m/z* 1570.6774. Melting points were determined using an Electrothermal IA9000 digital melting point apparatus.

General procedure for the synthesis of BTA amino acid methyl esters 14–17 (R and S)

Thionyl chloride (11 mol equiv) was added to a suspension of the amino acid (1 equiv) in CH_3OH at 0°C. The reaction mixture was allowed to reach room temperature and stirred for 6 h. After the reaction, CH_3OH and $SOCl_2$ were removed under reduced pressure to yield a solid of (*R/S*)-amino acid methyl ester hydrochloride, which was then used for further reaction without any purification. The (*R/S*)-amino acid methyl ester hydrochloride (1 equiv) was dissolved in CH_2Cl_2, and triethylamine was added to neutralize trace amounts

of $SOCl_2$ at 0°C. Then 1,3,5-benzene tricarbonyl trichloride (0.2 mol equiv) was added and the reaction mixture was stirred at room temperature for 12 h. Completion of the reaction was monitored by silica TLC using 94% CH_2Cl_2/CH_3OH. Once the reaction was complete, the reaction mixture was diluted with CH_2Cl_2 and washed with 1 M HCl, sat. $NaHCO_3$ solution, and H_2O. The CH_2Cl_2 layer was dried over Na_2SO_4, and the solvent was removed under reduced pressure to yield **14–17** (*R*/*S*). The crude products were purified using neutral silica column chromatography with 94% CH_2Cl_2/CH_3OH as mobile phase to yield the pure compounds **14–17**.

General procedure for the synthesis of BTA amino acids 18–21 (R and S)

To a suspension of compound **14–17** (*R*/*S*) (1 equiv) in CH_3OH, an aqueous solution of 1 M NaOH (5 equiv) was added at 0°C and this mixture was stirred at room temperature for 6 h. After completion of the reaction, NaOH was neutralized by adding Amberlite IR 120 H^+ resin until the pH reached 6.5. The resin was removed, and the liquid layer was evaporated under reduced pressure to obtain compounds **18–21** (*R*/*S*) as a white solid. These crude compounds were purified by re-precipitation in CH_3OH/Et_2O mixture to yield a white solid powder.

General procedure for the synthesis of tripodal BTA compounds 2–5 (R and S)

Compound **18–21** (*R*/*S*) was dissolved in a DMF/CH_2Cl_2 mixture (1:3 v/v) and cooled to 0°C in an ice/acetone bath. 1-Ethyl-3-(3-dimethylaminopropyl) carbodiimide (EDCI, 3.9 equiv) and 1-hydroxybenzotriazole (HOBt, 3.9 equiv) were added to this solution, and the resulting mixture was let to stir for 10 min. *N*-[2,2′;6′,2″]terpyridin-4′-yl-propane-1,3-diamine[32] was then added, and the mixture was allowed to reach room temperature and left stirring for 24 h. Once the reaction was complete, CH_2Cl_2 was removed under reduced pressure, and the remaining DMF was poured into ice cold water (~200 mL). The obtained white solid was filtered and dried under vacuum. The dried solid was dissolved in $CHCl_3$ and washed with sat. $NaHCO_3$ solution, H_2O and dried over Na_2SO_4. The solvent was removed under reduced pressure to yield crude tripodal BTA compounds (*R*/*S*). The crude compound was purified by column chromatography using neutral alumina as stationary phase and 90% $CHCl_3$/EtOH as mobile phase to yield the pure tripodal BTA compounds **2–5** (*R*/*S*).

Gelation tests

Gelation tests were carried out by dissolving a known amount (%, weight/volume) of the gelator in the respective solvent system in a test tube (*d*. 8 mm, *l*. 10 cm) by heating and followed by cooling to room temperature without any disturbance. If the liquid did not flow upon inverting the test tube, it was termed as a gel. Frequency sweep and strain sweep experiments were performed on the gels formed with compound **2**. Recovery tests were carried out by imposing an alternating low strain rate (0.1%, 1 Hz for 300 s) and a high strain rate (2,500%, 1 Hz for 300 s) during the first run of experiments and at low strain rate (0.1%, 1 Hz for 90 s) and a high strain rate (1,000%, 1 Hz for 90 s) during the second run of experiments.

Microscopy and spectroscopy methods

SEM was carried out with a Carl Zeiss ULTRA Plus field emission instrument using a beam current of 2–10 kV with an SE2 or InLens detector. The samples were smoothed (in the case of the gel) or dropcasted (in the case of the microspheres) on silica wafers and dried thoroughly. A gold coating was sputtered on the dried gel sample prior to recording the micrographs. TEM images were recorded using a titan FEI (Field Electron and Ion Company) TEM with an 80 kV beam current. FIB experiments were carried out using a Carl Zeiss Auriga FIB microscopy. An area was selected over the microspheres and milled with a beam of gallium ions with a current of 30 keV. The milled microspheres were imaged using SEM.[63] AFM-Raman spectroscopy was carried out using an NTEGRA Spectra AFM-Raman microscope, operating in tapping mode for AFM images and in tip enhanced Raman microscopy mode using a 514 nm laser for Raman imaging. Fluorescence confocal images for following the microsphere formation in real time were recorded using a Zeiss LSM 710 confocal microscope and the samples were excited by a continuous wave laser at λ_{ex} = 405 nm. Spectral reading and imaging has been done on a custom Zeiss Axiovert 200M microscope.[64] CPL spectra were recorded on a custom built spectrometer[55] using 365-nm LED excitation. All samples were prepared in HPLC or spectroscopic-grade solvents (THF, hexane, DMSO, MeOH, and water) with varying concentrations on the order of μM. UV-visible absorption spectra were recorded at 298 K in 1 cm quartz cuvettes on a Varian Cary 50 spectrophotometer. A baseline correction was applied for all spectra. Molar absorptivity determinations were verified by linear least-squares fit of values obtained from at least three independent solutions at varying concentrations ranging from 1.00×10^{-4} to 1.00×10^{-6} M.

RESOURCE AVAILABILITY

Lead contact

Further information and requests for resources should be directed to and will be fulfilled by the lead contact, Thorfinnur Gunnlaugsson (gunnlaut@tcd.ie).

Materials availability

All unique reagents generated in this study are available from the lead contact upon request.

Data and code availability

All data and code underpinning spectra presented herein are available from the lead contact upon request.

ACKNOWLEDGMENTS

Authors acknowledge the School of Chemistry TCD, Science Foundation Ireland (SFI PI awards 10/IN.1/B2999 and 13/IA/1865 to T.G., SFI CDA award 17/CDA/4704 to M.E.M.). T.G., M.E.M., and J.J.B. would also like to thank the SFI funded AMBER Centre for financial support (SFI 12/RC/2278_P2). E.T.L. would like to thank the Irish Research Council (IRC GOIPD/2020/585) for a Postdoctoral Fellowship. We thank the staff of the Advanced Microscopy Laboratory (AML) (part of the Centre for Research on Adaptive nanostructures and nanodevices [CRANN], TCD) for their support throughout this project. R.P. acknowledges support from the Royal Society University Research Fellowship URF\R\191002 and RF\ERE\210091, BBSRC BB/S017615/1 and BB/X001172/1, and EPSRC EP/X040259/1.

AUTHOR CONTRIBUTIONS

A.J.S., D.C.W., J.J.B., R.P., and T.G. conceived the idea. A.J.S., O.K., E.T.L., A.D.L., S.M., S.A.B., G.J.M., M.E.M., and R.P. designed and carried out the synthesis, designed and carried out the spectroscopic imaging, rheology, and other studies described. A.J.S., O.K., J.J.B., R.P., E.T.L., and T.G. co-wrote the manuscript. T.G., R.P., and J.J.B. provided expertise and feedback and provided SFI funding for the project.

DECLARATION OF INTERESTS

T.G. is a member of the *Chem* advisory board.

SUPPLEMENTAL INFORMATION

Supplemental information can be found online at https://doi.org/10.1016/j.chempr.2024.09.020.

Received: August 27, 2023
Revised: November 2, 2023
Accepted: September 19, 2024
Published: October 16, 2024

REFERENCES

1. Savyasachi, A.J., Kotova, O., Shanmugaraju, S., Bradberry, S.J., Ó'Máille, G.M., and Gunnlaugsson, T. (2017). Supramolecular Chemistry: A Toolkit for Soft Functional Materials and Organic Particles. Chem *3*, 764–811.
2. Agut, W., Brûlet, A., Schatz, C., Taton, D., and Lecommandoux, S. (2010). pH and temperature responsive polymeric micelles and polymersomes by self-assembly of poly[2-(dimethylamino)ethyl methacrylate]-b-poly(glutamic acid) double hydrophilic block copolymers. Langmuir *26*, 10546–10554.

3. Koide, A., Kishimura, A., Osada, K., Jang, W.D., Yamasaki, Y., and Kataoka, K. (2006). Semipermeable polymer vesicle (PICsome) self-assembled in aqueous medium from a pair of oppositely charged block copolymers: Physiologically stable micro-/nanocontainers of water-soluble macromolecules. J. Am. Chem. Soc. *128*, 5988–5989.
4. Du, X., Zhou, J., Shi, J., and Xu, B. (2015). Supramolecular Hydrogelators and Hydrogels: From Soft Matter to Molecular Biomaterials. Chem. Rev. *115*, 13165–13307.
5. Sang, Y., and Liu, M. (2019). Nanoarchitectonics through supramolecular gelation: Formation and switching of diverse nanostructures. Mol. Syst. Des. Eng. *4*, 11–28.
6. Han, W., Xiang, W., Li, Q., Zhang, H., Yang, Y., Shi, J., Ji, Y., Wang, S., Ji, X., Khashab, N.M., and Sessler, J.L. (2021). Water compatible supramolecular polymers: Recent progress. Chem. Soc. Rev. *50*, 10025–10043.
7. Dastidar, P. (2008). Supramolecular gelling agents: can they be designed? Chem. Soc. Rev. *37*, 2699–2715.
8. Weiss, R.G. (2014). The Past, Present, and Future of Molecular Gels. What is the status of the field, and where is it going? J. Am. Chem. Soc. *136*, 7519–7530.
9. Draper, E.R., and Adams, D.J. (2017). Low-Molecular-Weight Gels: The State of the Art. Chem *3*, 390–410.
10. Liu, M., Ouyang, G., Niu, D., and Sang, Y. (2018). Supramolecular gelatons: Towards the design of molecular gels. Org. Chem. Front. *5*, 2885–2900.
11. Schnitzer, T., Preuss, M.D., van Basten, J., Schoenmakers, S.M.C., Spiering, A.J.H., Vantomme, G., and Meijer, E.W. (2022). How Subtle Changes Can Make a Difference: Reproducibility in Complex Supramolecular Systems. Angew. Chem. Int. Ed. *61*, e202206738.
12. Zhang, L., Wang, X., Wang, T., and Liu, M. (2015). Tuning soft nanostructures in self-assembled supramolecular gels: From morphology control to morphology-dependent functions. Small *11*, 1025–1038.
13. Avinash, M.B., and Govindaraju, T. (2018). Architectonics: Design of Molecular Architecture for Functional Applications. Acc. Chem. Res. *51*, 414–426.
14. Webber, M.J., Appel, E.A., Meijer, E.W., and Langer, R. (2016). Supramolecular biomaterials. Nat. Mater. *15*, 13–26.
15. Onogi, S., Shigemitsu, H., Yoshii, T., Tanida, T., Ikeda, M., Kubota, R., and Hamachi, I. (2016). In situ real-time imaging of self-sorted supramolecular nanofibres. Nat. Chem. *8*, 743–752.
16. Wang, Y., Zhang, W., Gong, C., Liu, B., Li, Y., Wang, L., Su, Z., and Wei, G. (2020). Recent advances in the fabrication, functionalization, and bioapplications of peptide hydrogels. Soft Matter *16*, 10029–10045.
17. Johnson, E.K., Adams, D.J., and Cameron, P.J. (2011). Peptide based low molecular weight gelators. J. Mater. Chem. *21*, 2024–2027.
18. Tao, K., Levin, A., Adler-Abramovich, L., and Gazit, E. (2016). Fmoc-modified amino acids and short peptides: Simple bio-inspired building blocks for the fabrication of functional materials. Chem. Soc. Rev. *45*, 3935–3953.
19. Tang, C., Ulijn, R.V., and Saiani, A. (2011). Effect of glycine substitution on Fmoc-diphenylalanine self-assembly and gelation properties. Langmuir *27*, 14438–14449.
20. Lampel, A., McPhee, S.A., Park, H.A., Scott, G.G., Humagain, S., Hekstra, D.R., Yoo, B., Frederix, P.W.J.M., Li, T.D., Abzalimov, R.R., et al. (2017). Polymeric peptide pigments with sequence-encoded properties. Science *356*, 1064–1068.
21. Frkanec, L., and Žinić, M. (2010). Chiral bis(amino acid)- and bis(amino alcohol)-oxalamide gelators. Gelation properties, self-assembly motifs and chirality effects. Chem. Commun. *46*, 522–537.
22. Tomasini, C., and Castellucci, N. (2013). Peptides and peptidomimetics that behave as low molecular weight gelators. Chem. Soc. Rev. *42*, 156–172.
23. Huo, Y., Hu, J., Yin, Y., Liu, P., Cai, K., and Ji, W. (2023). Self-assembling peptide-based functional biomaterials. ChemBioChem *24*, 202200582.
24. Cantekin, S., de Greef, T.F.A., and Palmans, A.R.A. (2012). Benzene-1,3,5-tricarboxamide: A versatile ordering moiety for supramolecular chemistry. Chem. Soc. Rev. *41*, 6125–6137.
25. Aletti, A.B., Blasco, S., Aramballi, S.J., Kruger, P.E., and Gunnlaugsson, T. (2019). Sulfate-Templated 2D Anion-Layered Supramolecular Self-Assemblies. Chem *5*, 2617–2629.
26. Yang, Z., Altantzis, T., Zanaga, D., Bals, S., Van Tendeloo, G., and Pileni, M.P. (2016). Supracrystalline Colloidal Eggs: Epitaxial Growth and Freestanding Three-Dimensional Supracrystals in Nanoscaled Colloidosomes. J. Am. Chem. Soc. *138*, 3493–3500.
27. Albertazzi, L., Van Der Veeken, N., Baker, M.B., Palmans, A.R.A., and Meijer, E.W. (2015). Supramolecular copolymers with stimuli-responsive sequence control. Chem. Commun. *51*, 16166–16168.
28. Su, L., Mosquera, J., Mabesoone, M.F.J., Schoenmakers, S.M.C., Muller, C., Vleugels, M.E.J., Dhiman, S., Wijker, S., Palmans, A.R.A., and Meijer, E.W. (2022). Dilution-induced gel-sol-gel-sol transitions by competitive supramolecular pathways in water. Science *377*, 213–218.
29. Pandurangan, K., Kitchen, J.A., Blasco, S., Boyle, E.M., Fitzpatrick, B., Feeney, M., Kruger, P.E., and Gunnlaugsson, T. (2015). Unexpected self-sorting self-assembly formation of a [4:4] sulfate:ligand cage from a preorganized tripodal urea ligand. Angew. Chem. Int. Ed. *54*, 4566–4570.
30. Smulders, M.M.J., Schenning, A.P.H.J., and Meijer, E.W. (2008). Insight into the Mechanisms of Cooperative Self-Assembly: The "Sergeants-and-Soldiers" Principle of Chiral and Achiral C3-Symmetrical Discotic Triamides. J. Am. Chem. Soc. *130*, 606–611.
31. Kulkarni, C., Meijer, E.W., and Palmans, A.R.A. (2017). Cooperativity Scale: A Structure–Mechanism Correlation in the Self-Assembly of Benzene-1,3,5-tricarboxamides. Acc. Chem. Res. *50*, 1928–1936.
32. Kotova, O., Daly, R., dos Santos, C.M.G., Boese, M., Kruger, P.E., Boland, J.J., and Gunnlaugsson, T. (2012). Europium-Directed Self-Assembly of a Luminescent Supramolecular Gel from a Tripodal Terpyridine-Based Ligand. Angew. Chem. Int. Ed. *51*, 7208–7212.
33. Daly, R., Kotova, O., Boese, M., Gunnlaugsson, T., and Boland, J.J. (2013). Chemical nano-gardens: Growth of salt nanowires from supramolecular self-assembly gels. ACS Nano *7*, 4838–4845.
34. Martínez-Calvo, M., Kotova, O., Möbius, M.E., Bell, A.P., McCabe, T., Boland, J.J., and Gunnlaugsson, T. (2015). Healable luminescent self-assembly supramolecular metallogels possessing lanthanide (Eu/Tb) dependent rheological and morphological properties. J. Am. Chem. Soc. *137*, 1983–1992.
35. Kotova, O., Daly, R., dos Santos, C.M.G., Kruger, P.E., Boland, J.J., and Gunnlaugsson, T. (2015). Cross-Linking the Fibers of Supramolecular Gels Formed from a Tripodal Terpyridine Derived Ligand with d-Block Metal Ions. Inorg. Chem. *54*, 7735–7741.
36. Lynes, A.D., Hawes, C.S., Ward, E.N., Haffner, B., Möbius, M.E., Byrne, K., Schmitt, W., Pal, R., and Gunnlaugsson, T. (2017). Benzene-1,3,5-tricarboxamide n-alkyl ester and carboxylic acid derivatives: tuneable structural, morphological and thermal properties. CrystEngComm *19*, 1427–1438.
37. Lynes, A.D., Hawes, C.S., Byrne, K., Schmitt, W., and Gunnlaugsson, T. (2018). Coordination chemistry of flexible benzene-1,3,5-tricarboxamide derived carboxylates; Notable structural resilience and vaguely familiar packing motifs. Dalton Trans. *47*, 5259–5268.
38. de Loos, M., van Esch, J.H., Kellogg, R.M., and Feringa, B.L. (2007). C_3-Symmetric, amino acid based organogelators and thickeners: a systematic study of structure-property relations. Tetrahedron *63*, 7285–7301.
39. Veld, M.A.J., Haveman, D., Palmans, A.R.A., and Meijer, E.W. (2011). Sterically demanding benzene-1,3,5-tricarboxamides: Tuning the mechanisms of supramolecular polymerization and chiral amplification. Soft Matter *7*, 524–531.
40. Jana, P., Paikar, A., Bera, S., Maity, S.K., and Haldar, D. (2014). Porous organic material from discotic tricarboxyamide: side chain-core interactions. Org. Lett. *16*, 38–41.

41. Chen, W., Qing, G., and Sun, T.A. (2016). A Novel aggregation-induced emission enhancement triggered by the assembly of a chiral gelator: from non-emissive nanofibers to emissive micro-loops. Chem. Commun. *53*, 447–450.

42. Knoll, K., Leyendecker, M., and Thiele, C.M. (2019). L-valine derivatised 1,3,5-benzene-tricarboxamides as building blocks for a new supramolecular organogel-like alignment medium. Eur. J. Org. Chem. *2019*, 720–727.

43. Basuyaux, G., Desmarchelier, A., Gontard, G., Vanthuyne, N., Moussa, J., Amouri, H., Raynal, M., and Bouteiller, L. (2019). Extra hydrogen bonding interactions by peripheral indole groups stabilize benzene-1,3,5-tricarboxamide helical assemblies. Chem. Commun. *55*, 8548–8551.

44. Klein, T., Ulrich, H.F., Gruschwitz, F.V., Kuchenbrod, M.T., Takahashi, R., Fujii, S., Hoeppener, S., Nischang, I., Sakurai, K., and Brendel, J.C. (2020). Impact of amino acids on the aqueous self-assembly of benzenetrispeptides into supramolecular polymer bottlebrushes. Polym. Chem. *11*, 6763–6771.

45. Perlitius, F., Walczak, A., Čonková, M., Markiewicz, G., Harrowfield, J., and Stefankiewicz, A.R. (2022). Dimeric capsule vs columnar polymer: Structural factors determining the aggregation behavior of amino acid functionalized benzene-1,3,5-tricarboxamides in solution and in the solid-state. J. Mol. Liq. *367*, 120511.

46. Oh, M., and Mirkin, C.A. (2005). Chemically tailorable colloidal particles from infinite coordination polymers. Nature *438*, 651–654.

47. Masoomi, M.Y., and Morsali, A. (2013). Morphological study and potential applications of nano metal-organic coordination polymers. RSC Adv. *3*, 19191–19218.

48. Cho, W., Lee, H.J., Choi, S., Kim, Y., and Oh, M. (2014). Highly effective heterogeneous chemosensors of luminescent silica@coordination polymer core-shell micro-structures for metal ion sensing. Sci. Rep. *4*, 6518.

49. Lv, K., Zhang, L., and Liu, M. (2014). Self-assembly of triangular amphiphiles into diverse nano/microstructures and release behavior of the hollow sphere. Langmuir *30*, 9295–9302.

50. D'Amato, R., Medei, L., Venditti, I., Russo, M.V., and Falconieri, M. (2003). Chemical synthesis of polyphenylacetylene nanospheres with controlled dimensions for photonic crystals. Mater. Sci. Eng. C *23*, 861–865.

51. Freire, F., Seco, J.M., Quiñoá, E., and Riguera, R. (2012). Nanospheres with tunable size and chirality from helical polymer-metal complexes. J. Am. Chem. Soc. *134*, 19374–19383.

52. Aliprandi, A., Mauro, M., and De Cola, L. (2016). Controlling and imaging biomimetic self-assembly. Nat. Chem. *8*, 10–15.

53. Hartlieb, M., Mansfield, E.D.H., and Perrier, S.A. (2020). A Guide to supramolecular polymerizations. Polym. Chem. *11*, 1083–1110.

54. Zellmer, S., Garnweitner, G., Breinlinger, T., Kraft, T., and Schilde, C. (2015). Hierarchical Structure Formation of Nanoparticulate Spray-Dried Composite Aggregates. ACS Nano *9*, 10749–10757.

55. MacKenzie, L.E., Pålsson, L.O., Parker, D., Beeby, A., and Pal, R. (2020). Rapid time-resolved Circular Polarization Luminescence (CPL) emission spectroscopy. Nat. Commun. *11*, 1676.

56. Carr, R., Evans, N.H., and Parker, D. (2012). Lanthanide complexes as chiral probes exploiting circularly polarized luminescence. Chem. Soc. Rev. *41*, 7673–7686.

57. Zinna, F., and Di Bari, L. (2015). Lanthanide Circularly Polarized Luminescence: Bases and Applications. Chirality *27*, 1–13.

58. Godart, E., Della-Negra, O., Long, A., Insuasty, A., Arrico, L., Benetti, C., Antonetti, E., Nava, P., Cotelle, Y., Vanthuyne, N., et al. (2022). Circularly polarized luminescence of encaged Eu(III) and Tb(III) complexes controlled by an inherently chiral remote unit. New J. Chem. *46*, 20154–20159.

59. Kotova, O., O'Reilly, C., Barwich, S.T., Mackenzie, L.E., Lynes, A.D., Savyasachi, A.D., Ruether, M., Pal, R., Möbius, M.E., and Gunnlaugsson, T. (2022). Lanthanide luminescence from self-assembled supramolecular hydrogels consisting of bio-conjugated picolinic acid based guanosine quadruplexes. Chem *8*, 1395–1414.

60. Muller, G., and Riehl, J.P. (2005). Use of induced circularly polarized luminescence (CPL) from racemic D 3 lanthanide complexes to determine the absolute configuration of amino acids. J. Fluoresc. *15*, 553–558.

61. Binnemans, K. (2015). Interpretation of europium(III) spectra. Coord. Chem. Rev. *295*, 1–45.

62. Kim, C., Kim, K.Y., Lee, J.H., Ahn, J., Sakurai, K., Lee, S.S., and Jung, J.H. (2017). Chiral Supramolecular Gels with Lanthanide Ions: Correlation between Luminescence and Helical Pitch. ACS Appl. Mater. Interfaces *9*, 3799–3807.

63. Birch, R., Bruckbauer, J., Gajewska, M., Cios, G., Pal, R., and MacKenzie, L.E. (2023). Influence of polyvinylpyrrolidone (PVP) in the synthesis of luminescent NaYF4:Yb,Er upconversion nanoparticles. Methods Appl. Fluoresc. *11*, 034001.

64. Pal, R., and Beeby, A. (2014). Simple and versatile modifications allowing time gated spectral acquisition, imaging and lifetime profiling on conventional wide-field microscopes. Methods Appl. Fluoresc. *2*, 037001.